The effects of nonnative interactions on protein folding rates: Theory and simulation

CECILIA CLEMENTI[1,2] AND STEVEN S. PLOTKIN[3]

[1]Department of Chemistry, and W.M. Keck Center for Computational and Structural Biology, Rice University, Houston, Texas 77005, USA
[2]Structural and Computational Biology and Molecular Biophysics, Baylor College of Medicine, Houston, Texas 77030, USA
[3]Department of Physics and Astronomy, University of British Columbia, Vancouver, BC V6T1Z1, Canada

Abstract

Proteins are minimally frustrated polymers. However, for realistic protein models, nonnative interactions must be taken into account. In this paper, we analyze the effect of nonnative interactions on the folding rate and on the folding free energy barrier. We present an analytic theory to account for the modification on the free energy landscape upon introduction of nonnative contacts, added as a perturbation to the strong native interactions driving folding. Our theory predicts a rate-enhancement regime at fixed temperature, under the introduction of weak, nonnative interactions. We have thoroughly tested this theoretical prediction with simulations of a coarse-grained protein model, by using an off-lattice C_α model of the src-SH3 domain. The strong agreement between results from simulations and theory confirm the nontrivial result that a relatively small amount of nonnative interaction energy can actually assist the folding to the native structure.

Keywords: protein folding; frustration; free energy landscape; folding rate; minimalist model; molecular dynamics

Supplemental material: see www.proteinscience.org

The mechanism of protein folding is of central importance to structural and functional biology (see, e.g., Winkler and Gray 1998; Fersht 2000; Creighton 2002; Plotkin and Onuchic 2002a,b). An understanding of the fundamental physical–chemical factors regulating the folding process may help provide answers to some of the long-outstanding problems in both functional genomics and biotechnology: Rational design of drugs and enzymes, potential control of genetic diseases, and a deeper understanding of the connection between biological structure and function are among the applications that may benefit from advances in protein folding.

Theoretical and computational studies have recently achieved noticeable success in reproducing various features of the folding mechanisms of several small- to medium-sized fast-folding proteins (see, e.g., Shoemaker et al. 1999; Sorenson and Head-Gordon 2000, 2002; Shea and Brooks III 2001; Shimada and Shakhnovich 2002; Clementi et al. 2003; Karanicolas and Brooks 2003; Kaya and Chan 2003); at the same time, the improved spatial and temporal resolution of recent experimental techniques is now allowing researchers to combine theoretical and experimental data to give a more robust characterization of the folding free energy landscape (Lapidus et al. 2000; Ervin and Gruebele 2002; Schuler et al. 2002; Snow et al. 2002; Kubelka et al. 2003; Pande 2003). However, in spite of these recent successes, a microscopically detailed observation of the individual conformational motions that occur during folding remains elusive. Knowledge of the time-dependence of every degree of freedom in the system is, however, not of inherent interest, because no additional insight to the underlying physics of the folding process is gained from this

information by itself. Nor is any particular degree of freedom especially important to folding, because the transition involves the cooperation of many weakly (noncovalently) interacting constituents. For these reasons, a statistical description of the process of folding, in terms of the behavior of an ensemble of systems, is appropriate for distinguishing general (self-averaging) properties from sequence-specific ones (Bryngelson et al. 1995). The characterization of the folding process in statistical mechanical terms can pinpoint crucial questions that may be computationally or experimentally addressed in more detail.

The idea of considering ensemble properties to characterize the folding landscape underpinned studies of the transition state and folding mechanism as arising from the native-state topology (Shoemaker et al. 1997; Alm and Baker 1999; Galzitskaya and Finkelstein 1999; Munoz and Eaton 1999; Clementi et al. 2000a,b, 2001, 2003; Shea et al. 2000). As a general rule, the transition-state structure does not differ dramatically between homologous proteins (Baker 2000; Plaxco et al. 2000a; Gunasekaran et al. 2001), and any exceptions are fairly readily explained (Ferguson et al. 1999; Kim et al. 2000). Consistent with the above-mentioned notion of self-averaging, folding rates of homologous proteins are seldom seen to differ by more than an order of magnitude when tuned to the same stability (Mines et al. 1996; Plaxco et al. 2000b). This indicates that the folding free energy barrier is not particularly sensitive to the details of sequences folding to a given native structure, but depends rather on more general features of that ensemble of sequences, including the kinetic accessibility of that native structure. In this sense, the topology of the native structure largely determines the folding free energy barrier for those homologous sequences (Plaxco et al. 2000b).

These ideas motivated many studies of folding rates and mechanisms using so-called Gō models (Ueda et al. 1975), which neglect interactions not present in the native state. In these studies, the possibility of structure prediction is traded for the possibility of rate and mechanism prediction. Moreover, because of the robustness of rate and mechanism for homologous proteins, the coarse graining of the Gō model (i.e., removing the molecular details of side chains and solvent) is often assumed a reasonable approximation.

Topology-based approaches seek to predict mechanism by calculating φ-values (Fersht et al. 1986; Matouschek et al. 1990) or analogous quantities, which in an accurate theory give values that correlate with experiment for the measured cases. Occasionally one finds residues whose φ-values are negative. This is most likely caused by the presence of nonnative contacts that stabilize the transition state, but cannot be present in the native state. The presence of nonnative interactions in the transition state is supported by all-atom simulations using a Charmm-based effective energy function, where it was found that ~20%–25% of the energy in the transition state arose from nonnative contacts (Paci et al. 2002).

Hence, for a more realistic protein potential energy function, nonnative interactions must be taken into account. In this paper, we analyze the effect of increasing the strength of nonnative interactions on the folding rate as well as the free energy barrier. Nonnative interactions are introduced as additional contacts between pairs of residues not in contact in the native structure, which are allowed to have a nonzero mean and a nonzero variance. The nonnative interactions are added perturbatively to the Gō model: All nonnative contacts are given a random energy with mean ϵ_{NN} and a variance b^2, which is progressively increased to examine more frustrated proteins, while the native contact energies are all held fixed to the same number. The limiting case of $\epsilon_{NN} = 0$ and $b = 0$ corresponds to the plain Gō model. This procedure essentially preserves the stability of the native state, where approximately no nonnative interactions are present. However, the stability of the unfolded state is lowered (as shown below).

At first glance, one would expect that introducing progressively larger nonnative contact energies to an otherwise energetically unfrustrated Gō protein would slow the folding rate, for straightforward reasons: It would seem that "noise" in the system would make the native basin harder to recognize. One might argue by analogy that it is easier to read a page of text without random misspellings. However, the folding rate has been predicted to initially increase under the introduction of weak, nonnative interactions, added as a perturbation to the strong native interactions driving folding (Plotkin 2001). This was a fold-independent result derived from general principles of energy landscape theory. This prediction was subsequently verified in simulations of a 36-mer lattice model (Fan et al. 2002), as well as off-lattice molecular dynamics simulations of Crambin, in which attractive nonnative contacts were successively added (Cieplak and Hoang 2002). Independently, it was found that nonnative interactions were present in the transition state of a 28-mer lattice-model protein with side chains, and increased the folding rate when strengthened (Li et al. 2000). Similar observations were also seen in two-dimensional 24-mer lattice models (Treptow et al. 2002). A different computational study on a 36-mer lattice-model protein found that at the temperature of fastest folding in simulation models, the folding rate monotonically decreases with increasing ruggedness (Fan et al. 2002; the temperature of fastest folding, of course, varies with the ruggedness). However, this typically barrierless regime is rarely seen in the laboratory (Gruebele 1999; Sabelko et al. 1999).

The prediction that strengthening nonnative interactions that were initially weak would accelerate folding is also consistent with experimental observations that strengthening nonspecific hydrophobic stabilization in the α-spectrin Src homology 3 (SH3) domain sped up folding (and unfold-

ing) for that protein (Viguera et al. 2002). This result was significantly nontrivial, to the extent that the experimental observation was originally interpreted (mistakenly) as evidence against the energy landscape theory.

In this paper, we test this prediction with simulations of a coarse-grained protein model, by using an off-lattice C_α model (see e.g., Honeycutt and Thirumalai 1992; Clementi et al. 2000b) of the SH3 domain of src tyrosine-protein kinase (src SH3). We use a Hamiltonian function that has tunable amounts of nonnative energy (see Supplemental Material for details). The results from simulations are compared with the predictions of an improved version of the existing theory (Plotkin 2001). The theory is improved by introducing a finite-size treatment of packing fraction as a function of polymer length, which takes better account of the polymer physics involved in collapse as folding progresses. Moreover, the previous study treated the rate enhancement at fixed stability. Here, we show a perhaps even less intuitive result, namely, that the rate enhancement can happen at fixed temperature, and we derive the conditions required for this to happen.

As the strength of nonnative interactions is increased to larger values, we find that eventually the folding rate decreases drastically, as expected. In the limit of large nonnative contact energies, the chain behaves like a random heteropolymer, having misfolded structures more stable than the native state.

The folding mechanism is also nontrivially affected by the introduction of nonnative interactions. In this regard, the analysis of the robustness of the folding mechanism against an increasingly strong perturbation on the nonnative interactions can provide a critical assessment on the validity of unfrustrated protein models for the prediction of folding mechanism, for different protein topologies. This analysis goes beyond the scope of the present paper, and it will be addressed separately (S.S. Plotkin and C. Clementi, unpubl.).

The paper is organized as follows: In the next section, we present the theory. After presenting the general ideas and overall strategy, we discuss in detail how an explicit expression for the conformational entropy can be obtained in terms of the packing fraction. We then use this result to show how the thermodynamic free energy barrier is lowered by the presence of nonnative interactions. In the third section, we test the theoretical predictions with direct simulation of the src-SH3 domain. We first compare the definition of reaction coordinates and the relative approximations of theory and simulations; thermodynamic and kinetic quantities obtained from simulations are then quantitatively compared with the corresponding theoretical predictions.

The strong agreement between results from simulations and theory confirms the nontrivial result that a relatively small amount of nonnative interaction energy can actually assist the folding to the native structure.

Theory of folding with nonnative interactions

Definition of the general strategy

Thermodynamic quantities relevant to folding may be obtained from an analysis of the density of states in the presence of energetic correlations (Plotkin and Onuchic 2002a,b). In this context, we introduce two order parameters. We let Q be the fraction of contacts shared between an arbitrary structure and the native structure, and we let A be the fraction of possible nonnative contacts present in that structure, that is, the number of nonnative contacts divided by the total possible number of nonnative contacts. These two order parameters are natural for the study of nonnative interactions in protein folding. Both take on values between zero and unity.

There are several relevant energy and entropy scales governing the thermodynamics of folding. Let the energy of the native structure be given by E_N. Let the total number of contact interactions in a fully collapsed polymer globule be given by M. Asymptotically, M scales like the total number of residues in the chain, N, essentially because surface terms are negligible compared with the bulk. However, for a finite-size system, the mean number of contacts per residue (native or nonnative), that is, the coordination number z, is itself a function of N. We can write the native energy as

$$E_N = M\epsilon = zN\epsilon, \qquad (1)$$

where ϵ is then defined as the mean native attraction energy ϵ ($\epsilon < 0$); that is, the native state is assumed to be fully collapsed with the maximal number of contacts, and this is the maximal number of total contacts of a fully collapsed polymer globule. We neglect here the separate effects that arise from the variance in the native interaction energies: $\delta\epsilon^2 = 0$.

Let the conformational entropy of an ensemble of polymer structures characterized by the order parameters Q and A be given by $S_c(Q,A)$. We can write the entropy in terms of the entropy per residue $s_c(Q,A)$ as:

$$S_c(Q,A) = Ns_c(Q,A) = Ms_c(Q,A)/z. \qquad (2)$$

In addition to the energy scales ϵ and $\delta\epsilon^2$ governing native contacts, there are also two energy scales governing nonnative interactions. One is the mean energy of a nonnative interaction ϵ_{NN}, and the other is the energetic variance of nonnative interactions b^2. We keep both of these terms, as they enter the analysis on essentially the same footing. For configurations with MA nonnative contacts, the total nonnative energy is taken to be Gaussianly distributed with mean $MA\epsilon_{NN}$ and variance MAb^2. Both of these terms contribute to the overall ruggedness of the energy landscape by favoring nonnative configurations.

The strength of nonnative interactions is taken to be weak, so that

$$b/\epsilon \ll 1 \qquad (3a)$$

$$\epsilon_{NN}/\epsilon \ll 1 \qquad (3b)$$

are both satisfied. Condition 3a implies that the ratio of the folding transition temperature T_F to the thermodynamic glass temperature T_G is large (Goldstein et al. 1992),

$$T_F/T_G \gg 1, \qquad (4)$$

that is, the proteins we consider are strongly (but not infinitely) unfrustrated—we are perturbing away from the Gō model. Condition 3b implies that collapse and folding occur concurrently (Klimov and Thirumalai 1996), that is,

$$T_F/T_\theta \gg 1, \qquad (5)$$

where T_θ is the temperature below which nonnative states tend to be collapsed. For a given choice of nonnative interaction energies, the energies of configurations for the ensemble of states characterized by (Q,A) is assumed Gaussianly distributed with a mean of $QM\epsilon + AM\epsilon_{NN}$ and a variance of AMb^2. Then the extensive part of the log number of states having energy E and order parameters (Q,A) is given by:

$$\log n(E,Q,A) = S_c(Q,A) - \frac{[E - (QM\epsilon + AM\epsilon_{NN})]^2}{2AMb^2}. \qquad (6)$$

From the definition of equilibrium temperature $T^{-1} = \partial S/\partial E$, one can then find the thermal energy, entropy, and free energy, which are given by (in units where $k_B = 1$):

$$\frac{E(Q,A,T)}{M} = \epsilon Q + \left(\epsilon_{NN} - \frac{b^2}{T}\right)A \qquad (7a)$$

$$\frac{S(Q,A,T)}{M} = \frac{s_c(Q,A)}{z} - \left(\frac{b^2}{2T^2}\right)A \qquad (7b)$$

$$\frac{F(Q,A,T)}{M} = \epsilon Q - T\frac{s_c(Q,A)}{z} + \left(\epsilon_{NN} - \frac{b^2}{2T}\right)A. \qquad (7c)$$

These expressions can be understood straightforwardly. In the absence of nonnative interactions ($\epsilon_{NN} = b = 0$), the thermal energy is just the energy of native contacts times the

number of native contacts, and the entropy is just the configurational entropy. When nonnative energies are present, just as ϵ couples the order parameter Q, so does ϵ_{NN} couple the order parameter A. When nonnative energies have a variance, the lower energy conformations (with stronger nonnative contacts) tend to be thermally occupied. This is why ϵ_{NN} and $-b^2/T$ enter on the same footing in the energy. The fact that the system spends more time in fewer states means that the thermal entropy is reduced. However, the entropy (times temperature) is only reduced by half as much as the energy, so that there is a residual contribution to the free energy $E - TS$ due to the variance of nonnative interactions.

A plot of the free energy at the folding temperature of the Gō model T_F° as a function of (Q,A) is shown in the first row of Figure 1, for equation 7c together with the analytical model of the configurational entropy $S_C(Q,A)$ described below.

Figure 1 also shows plots of $E(Q,A)$, $S(Q,A)$, and $F(Q,A)$, as well as the number of states at energy E, taken from the simulation data for the off-lattice model (see below). Plots are at the folding temperature T_F° of the Gō model, for several different values of b indicated.

Conformational entropy in terms of packing fraction

The fraction of nonnative contacts A is not independent of Q. As more native interactions are present, less nonnative interactions are allowable, and eventually there can be no nonnative contacts in the native structure. Previous studies that investigated the folding rate at fixed stability have explicitly included this Q-dependence in equation 7c (Plotkin 2001). Here, our intention is to plot the folding rate at fixed temperature rather than at fixed stability. For this purpose, it is formally more convenient to keep this Q-dependence implicit in A. Again this manifests itself only as a region of allowed values of (Q,A), which can be seen in Figure 1.

The entropy loss due to native contacts is of a different functional form than the entropy loss due to nonnative contacts. The entropy loss caused by native contacts arises from a specific set of polymeric constraints. The entropy loss caused by nonnative contact formation arises from an increase in polymer density, a nonspecific constraint. There are many collapsed unfolded states with nonnative interactions present, but only one folded state (neglecting the much smaller entropy caused by native conformational fluctuations).

We note that the conformational entropy $S_C(Q,A)$ takes into account the extent to which polymer configurations tend to have residue pairs in proximity, such that if they interacted, that interaction would be considered a nonnative contact. However, the strength of the typical nonnative interaction ($\sim\epsilon_{NN} \pm b$) is controlled by two free parameters in the theory. When both ϵ_{NN} and b are set to zero, the thermal
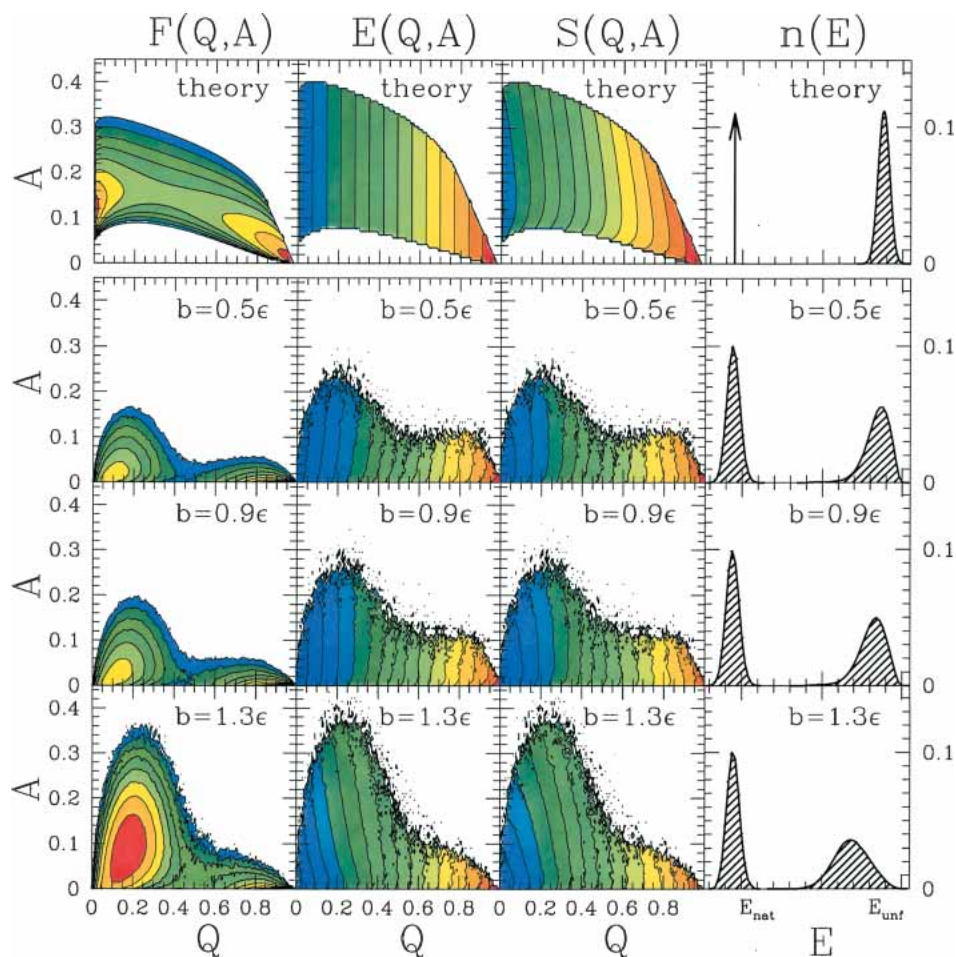
Figure 1. Free energy (first column from the *left*), energy (second column), and entropy (third column) surfaces as functions of the fraction Q of native contacts, and the fraction A of nonnative contacts, as obtained from theory and simulations. Also shown is the fraction of states, $n(E)$, populated as a function of the energy E. The distribution of the energy in the unfolded ensemble is shown, along with the distribution in the native state (fourth column). The distribution $n(E)$ is normalized; that is, the integral of $n(E)$ over all energies is 1 in all the cases plotted here. All free energy contours are spaced at ~1ϵ (where ϵ is the energy per native contact). Values of the parameters are given in Table 1. (*Top* row) Theoretical free energy, energy, and entropy surface at the folding temperature, obtained from equation 7c and equation A.16 in the Supplemental Material with all parameters set equal to the corresponding simulation values (see Table 1) and $b_{\text{theory}} = 0.3\epsilon$, where ϵ is the energy per native contact (this corresponds to $0.9\epsilon < b < 1.3\epsilon$ in the simulations; see text for detail). The transition state has more nonnative contacts than the unfolded state. The difference in the theoretical model is $\Delta A\ddagger \sim 0.035$. This amounts to an increase in the total number of nonnative contacts of $MA \sim 5$. The barrier height is ~$3.47\epsilon \sim 3.3 k_B T_f$. (*Bottom* three rows) Corresponding results obtained from simulations, for three different values of the nonnative energy perturbation parameter b: $b = 0.5\epsilon$ (second row), $b = 0.9\epsilon$ (third row), and $b = 1.3\epsilon$ (bottom row). The barrier heights and values of $\Delta A\ddagger$ obtained in simulations are plotted in Figure 10 as a function of the nonnative energy perturbation parameter b.

entropy reduces to that of the putative Gō model, with the configurational entropy $S_C(Q,A)$ remaining unchanged.

The A-dependence in $S_C(Q,A)$ is related to the physics of collapse, because at a given value of Q, the fraction of nonnative contacts A depends on the packing fraction η of nonnative polymer. When MQ native contacts are present, $A_{\text{MAX}} \equiv M(1 - Q)$ nonnative contacts are allowable, and A_{MAX} nonnative contacts are present when $\eta = 1$.

As detailed in the Supplemental Material, a mean field approximation allows one to estimate the conformational

entropy $S_c(Q,\eta)$ of a disordered polymer at Q with packing fraction η as:

$$S_c(Q,\eta) = N(1-Q)\left\{ \ln\frac{v}{e} - \left(\frac{1-\eta}{\eta}\right) \ln(1-\eta) \right.$$
$$\left. -\frac{1}{6}\left[\left(\frac{\overline{\eta}(Q)}{\eta}\right)^{2/3} - 1 \right]^2 \right\}$$
$$\equiv N(1-Q)s_{nn}(Q,\eta). \tag{8}$$

Here $\overline{\eta}(Q) = \overline{\ell}(Q)^{-1/2} = [n_L(Q)/N(1 - Q)]^{1/2}$, where $\overline{\ell}$ is the mean loop length formed by native contacts at Q (see

equation A.14 in the Supplemental Material), and $n_L(Q)$ is the total number of loops at Q (see equation A.15 in the Supplemental Material). In equation 8, the quantity in curly brackets is the entropy per residue for the remaining disordered polymer at Q.

Figure 2 shows a plot of the entropy per disordered residue at Q, $s_{nn}(Q,\eta) = S(Q,\eta)/N(1-Q)$, as a function of η, for various values of Q. This shows that the nonnative polymer density where most of the states are [where $s_{nn}(\eta)$ is maximal] is an increasing function of nativeness, Q.

From equations 2 and 8,

$$s_c(Q,A) = (1-Q)s_{nn}(Q,A/(1-Q)) \qquad (9)$$

The entropy per residue $s_c(Q,A)$ in equation 7b is then obtained from equation 8 using

$$s_c(Q,A) = s_c(Q,\eta)|_{\eta=A/(1-Q)} \qquad (10)$$

(see equation A.3 in the Supplemental Material). The free energy surface on which dynamics occurs can then be obtained from equation 7c, and is plotted in the first row of Figure 1. This is the reaction surface for the coordinates (Q,A).

Effect of nonnative interactions on the free energy barrier and folding rate

In the Gō model, nonnative contacts are given coupling energies of zero. The Gō folding temperature $T_F°$ is taken to be the temperature at which the unfolded and folded thermodynamic states have equal probability. This is given through equation 7c when $F(0,A) \approx F(1,0)$ and

$$\frac{S(\eta,Q)}{N(1-Q)} \quad \text{(Entropy per unfolded residue)}$$
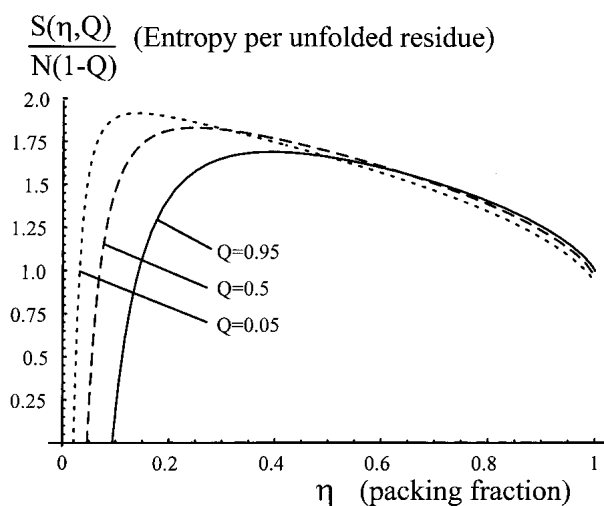
Figure 2. The entropy per residue $s_{nn}(Q,\eta) = S_c(q,\eta)/N(1-Q)$ in equation A.16 in the Supplemental Material, for the disordered part of a protein of nativeness Q, as a function of the disordered polymer's packing fraction η.

$\epsilon_{NN} = b^2 = 0$. We are taking $Q \approx 0$ in the unfolded state and $A = 0$ in the folded state (see Fig. 1). This yields a Gō folding temperature of

$$T_F^o = \frac{z|\epsilon|}{s_c(0, A*(0))} \qquad (11)$$

where $A*(Q)$ is the most probable value of A at a given Q, as determined below.

When considering the simulation data, the folding temperature is taken to be the temperature in the Gō model at which the unfolded and folded thermodynamic minima have equal free energies (these minima need not be precisely at $Q = 0$ and $Q = 1$).

The most probable value of A at a given Q for a protein in thermal equilibrium, $A*(Q)$, is obtained from:

$$\left.\frac{\partial F(Q,A)}{\partial A*}\right|_Q = 0. \qquad (12)$$

Using equations 7c and 8 this gives

$$\frac{\partial s_{nn}(Q,\eta*)}{\partial \eta} = \frac{z\epsilon_{NN}}{T} - \frac{zb^2}{2T^2}. \qquad (13)$$

where $\eta*(Q)$ is the most probable packing fraction at a given value of Q.

Using the following definitions,

$$\Delta A*(Q) \equiv A*(Q) - A*(0),$$

$$\Delta s_{nn}(Q) \equiv s_{nn}(Q,A*(Q)) - s_{nn}(0,A*(0)),$$

the minimal free energy at Q, $F(Q,A*(Q))$, relative to the minimal free energy $F(0,A*(0))$ in the unfolded state, is obtained from equation 7c:

$$\Delta F(Q,T) \equiv F(Q,A*(Q), T) - F(0,A*(0), T) \qquad (14)$$

$$\frac{\Delta F(Q,T)}{M} = Q\left(\epsilon + \frac{Ts_{nn}(0,A*(0))}{z}\right) - \frac{T(1-Q)\Delta s_{nn}(Q)}{z}$$
$$+ \left(\epsilon_{NN} - \frac{b^2}{2T}\right)\Delta A*(Q) \qquad (15)$$

With the temperature set to the Gō transition temperature $T_F°$, the first term in brackets in equation 15 vanishes. The free energy barrier (over $T_F°$) at the Gō transition temperature can then be written as

$$\frac{\Delta F^{\neq}}{T_F^o} = \frac{\Delta F^{o\neq}}{T_F^o} + M\left(\frac{\epsilon_{NN}}{T_F^o} - \frac{b^2}{2T_F^{o2}}\right)\Delta A*(Q^{\neq}) \qquad (16)$$

where $\Delta F^{\circ\neq}$ is the barrier height at T_F° with $\epsilon_{NN} = b^2 = 0$, that is, the putative Gō barrier height, and is given by

$$\frac{\Delta F^{o\neq}}{T_F^o} = N(1 - Q^\neq)(-\Delta s_{nn}(Q^\neq)) \qquad (17)$$

where the saddle point is located at $(Q^\neq, A^\neq \equiv A^*(Q^\neq))$. Note that $\Delta s_{nn}(Q) < 0$ because disordered polymer dressing larger native cores is more collapsed than that for smaller native cores. One can see that the barriers scale extensively as a result of the mean field approximations made above.

Thus we see from equation 16 that the folding barrier lowers with increasing nonnative interaction strength, namely, if $\epsilon_{NN} < 0$ $(b^2 > 0$ always), so long as $\Delta A^*(Q^\neq) \equiv \Delta A^\neq > 0$. We therefore investigate the conditions for which $\Delta A^\neq > 0$.

From equation A.1 in the Supplemental Material, the condition $\Delta A^\neq > 0$ is equivalent to

$$\Delta A^\neq = \eta^*(Q^\neq)(1 - Q^\neq) - \eta(0) > 0 \qquad (18)$$

where η^* is determined from equation 13.

We are interested in the effect on the barrier when nonnative interactions are imagined to initially increase from zero. For ϵ_{NN}, $b \approx 0$, the most probable packing fraction is interpreted geometrically through equation 13 as the value of η where the entropy per disordered residue is maximal, that is, the maximum of the curves in Figure 2. When $\epsilon_{NN} < 0$ and/or $b > 0$, η^* is determined as the value of η slightly to the right of the maximum in the curves in Figure
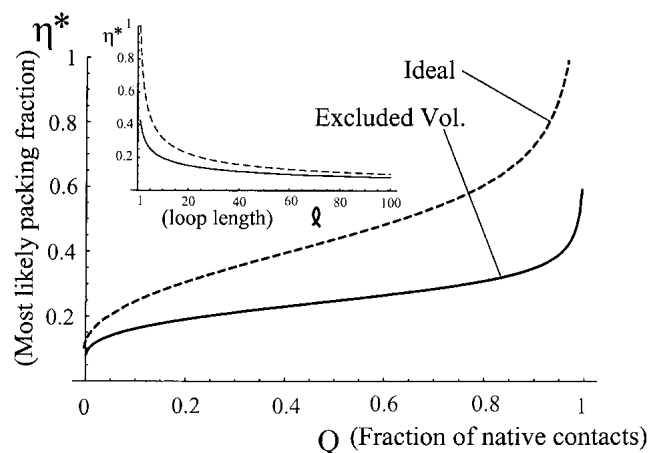
Figure 3. The most probable packing fraction η^* is a monotonically increasing function of nativeness Q. The dashed curve shows the characteristic packing fraction when the disordered loops are assumed to obey ideal chain statistics. The solid curve accounts for the effects of excluded volume, which are included in equation 8. (*Inset*) The most probable packing fraction is a decreasing function of the mean disordered loop length ℓ in equation A.14 in the Supplemental Material.
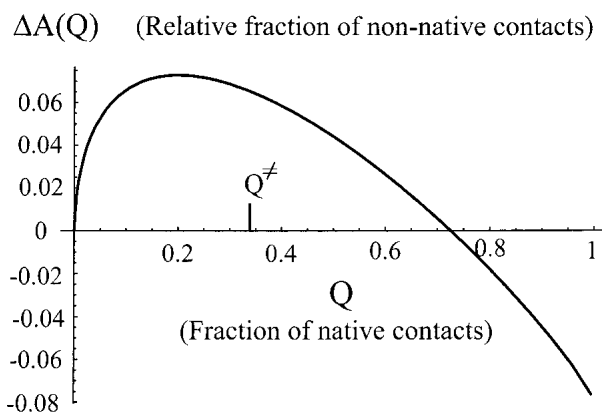
Figure 4. Fractional change in the number of nonnative interactions as a function of nativeness Q, for the theoretical model. We can see that the number of nonnative interactions initially increases before decreasing. For the model considered here, the barrier position $Q^\neq$ is well within this region of values where the number of nonnative interactions has increased. There are generically more nonnative interactions present in the transition state than in the unfolded state, for strongly minimally frustrated proteins. The effect is fairly modest—for a 100-residue protein, there are about six more nonnative interactions in the transition state. The shape of the curve is obtained from setting $\partial F/\partial A|_Q = 0$ in the first row of Figure 1.

2. The most probable packing fraction as a function of Q is plotted in Figure 3.

Equation 18 is not a particularly robust condition. Whereas $\eta^*(Q)$ is certainly a monotonically increasing function of Q as can be seen from Figure 3, the factor of $(1 - Q)$ in equation 18 de-emphasizes, or may reverse, the trend in $A^*(Q)$. In the earlier work addressing the trend in rates at fixed stability rather than fixed temperature, the factor determining whether rates would increase was merely the increase in packing fraction $\Delta\eta(Q)$ by itself (Plotkin 2001).

The derivative of s_{nn} in equation 13 can be straightforwardly determined from equation 8, and equation 13 then becomes a nonlinear equation for $\eta^*(Q)$ that can be solved numerically. The result is shown in Figure 3. The packing fraction increases as the length of disordered loops becomes shorter (inset of Fig. 3), and thus increases monotonically with nativeness Q.

Once $\eta^*(Q)$ is known, $\Delta A^*(Q)$ can be obtained from equation 18. This determines the trend in the barrier height in equation 16. A plot of $\Delta A^*(Q)$ is shown in Figure 4. We can see that if the barrier position $Q^\neq$ resides in a window of Q where $\Delta A(Q) > 0$, the barrier decreases with increasing nonnative interaction strength, for weak nonnative interactions. Otherwise, the barrier increases with increasing nonnative interaction strength.

When nonnative interactions are weak, the folding kinetics are single exponential:

$$k_F = k_o(\epsilon_{NN}, b)e^{-\Delta F^\neq(\epsilon, \epsilon_{NN}, b)/T}. \qquad (19)$$

Increasing the strength of nonnative interactions slows the prefactor k_0, owing to the effects of transient trapping. However, as ϵ_{NN} and b are increased from zero, this slowing effect on k_0 does not become significant until a nonzero characteristic value, which would indicate the onset of a dynamic glass transition in an infinite-sized system (see Takada et al. 1997; Wang et al. 1997; Eastwood and Wolynes 2001; Plotkin 2001 for more detailed treatments of this effect). In a finite system, the activation time $\sim k_0^{-1}$ increases dramatically but only when $b > b_A$ or $\epsilon_{NN} > \epsilon_{NN}^A$. The values of the energy scales b_A and ϵ_{NN}^A are of order T, thus there is a fairly large window upon increasing b, ϵ_{NN} from zero where the prefactor k_0 is unaffected to the first approximation. In this regime, the effects on rate are governed solely by the effects on barrier height. Hence, the decrease in barrier height shown above as ϵ_{NN}, b are increased from zero may be associated with an increase in folding rate.

In the next section we test the theoretical prediction directly with simulations of a model protein. The upshot is shown in Figure 10, B and C (below), which shows, indeed, an increase in folding rate with increasing nonnative interaction strength.

Comparison between theoretical prediction and simulation results

We have thoroughly explored the range of validity of the approximations made in the analytic theory by comparing the predictions with the results obtained from simulations on a Gō model increasingly perturbed by the addition of nonnative interactions (see Supplemental Material for details on simulation).

A close and quantitative comparison of the results from theory and simulations is possible if corresponding thermodynamic quantities and reaction coordinates are identified. For this purpose, before we proceed to test the prediction on rate enhancement, three main points of the theory have to be examined in comparison with the results from simulations:

- definition of the reaction coordinates Q and A;
- allowed values of the reaction coordinates (i.e., correlation between Q and A);
- approximations made in the definition of energy and entropy as functions of the reaction coordinates.

These points are clearly interconnected, and all affect the detailed shape of the free energy landscape, the value of the folding temperature, and the identification of the folded, unfolded, and transition state ensembles. We expect that the assumptions we have made in the analytical theory do not qualitatively change the theoretical predictions; nevertheless, a careful dissection of the basic ingredients we have used is needed for a quantitative assessment of the results.

In the following, we discuss in detail each of the points above. Unless otherwise specified, the following results are all obtained from simulations at the Gō folding temperature T_f°, for all values of b/ϵ.

Definition of reaction coordinates

The reaction coordinate Q, defined as the fraction of native contacts formed in a given protein configuration, is readily associated to configurations sampled by simulations (see Supplemental Material). More care has to be used in transposing the other reaction coordinate we have used in the theory, A (defined as the fraction of nonnative contacts formed), to the analysis of simulations data. In the analytical theory, we have assumed that the maximum number of nonnative contacts that can be formed at a certain stage of the folding reaction does not depend on the perturbation strength, and is a function of the degree of nativeness, Q, that is, $A_{max}(Q) = 1 - Q$, $\forall b$ (see equation A.1 in the Supplemental Material). This implies that no nonnative contacts can be formed in the native state ($A_{max} \sim 0$ if $Q \sim 1$), and vice versa ($A_{max} \sim 1$ if $Q \sim 0$). This assumption in the theory allows us to simplify the analytical calculations but does not qualitatively affect the results. The dependence on Q of the maximum number of nonnative contacts can be directly checked in simulations. In this regard, an important difference between theory and simulations is that a certain number (typically ~ 5) of nonnative contacts can be accommodated in a protein configuration with $Q \sim 1$ and minimal (<1 Å) RMSD from the PDB native structure. The increased number of contacts around the native configurations arises mainly from the fact that native or nonnative contacts are considered formed in a small but finite length range (typically ~ 1 Å) around the minimum of the interaction potential. This leads to probable formation of some nonnative contacts as the protein undergoes fluctuations around the native state.

Figure 5 shows that a subset of six nonnative contacts is formed with probability >0.25 in the native state ensemble for $b/\epsilon = 1.3$. Similar results are obtained for all values of b/ϵ used in this study, although the particular set of nonnative contacts formed in each case depends on the choice of nonnative interactions (data not shown).

Contacts that are easily formed in the native state cannot be considered nonnative, even when they are not listed as native contacts in the unperturbed Gō-like Hamiltonian. In fact, contacts that can be made in the native state are not competing against the formation of the native structure; rather, they are assisting it. To remove this effect, we introduce a new reaction coordinate A', defined as the fraction of nonnative contacts formed, restricting the list of nonnative interactions only to the ones with a probability of contact formation in the native state ensemble smaller than a cutoff value p_c. The native ensemble for each sequence is identified as all configurations with $Q > 0.9$ sampled in
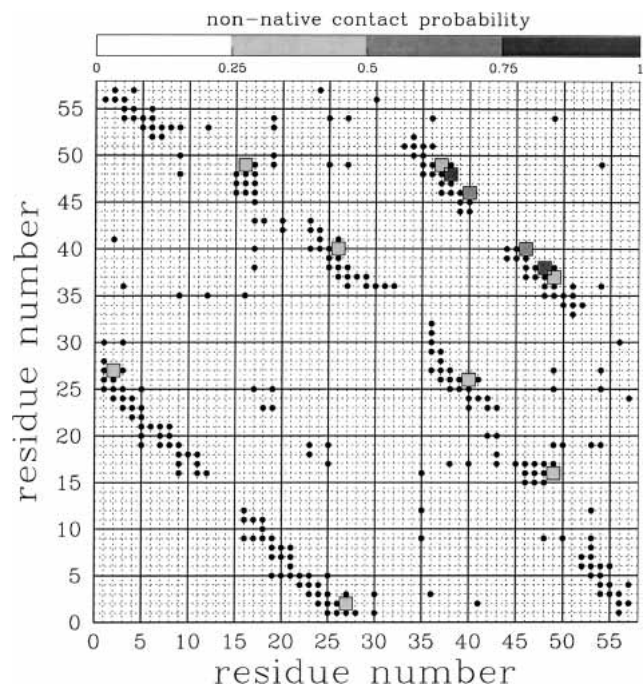
Figure 5. Probability of formation of nonnative contacts in the native configuration of SH3. Black dots in the contact map represent native contacts, whereas nonnative contacts formed with probability >0.25 are shown with probabilities given by the gray scale on *top*. Probability values are computed by averaging the formation of nonnative contacts over ≳50,000 configurations with $Q > 0.9$ from folding/unfolding simulations. The data shown in this figure are for a nonnative perturbation strength $b/\epsilon = 1.3$. Similar results are obtained for different values of the parameter b (see Fig. 6).

simulation for that sequence. The results presented in the following are all obtained with a probability cutoff $p_c = 0.1$. Smaller values of p_c yield essentially the same results. The reaction coordinate A' is then used in this study to compare results from simulation with the theoretical predictions.

Another approximation that can be directly checked in simulation is on the maximum number of nonnative contacts that can be formed at different stages of the folding reaction. In the analytical theory, the fraction of nonnative contacts, A, is a function of the fraction of native contacts formed in a configuration, Q, and of the packing fraction η of the nonnative part of the protein: $MA = \eta(1 - Q)M$ (see equation A.1 in the Supplemental Material), with $0 \leq \eta \leq 1, \forall Q$. The maximum number of nonnative contacts is then $A_{max}M = (1 - Q)M$, and the maximum total fraction of all contacts (native and nonnative) is $(A + Q)_{max} = 1, \forall Q$. Indeed, the maximum number of all contacts (both native and nonnative) recorded in simulations is close to the number of native contacts formed in the native state, that is, $M(Q + A')_{max} \simeq M$, for all values of the parameter b examined in this study (see Fig. 6A). Figure 6B shows the behavior of the average number of nonnative

contacts formed in simulation (both coordinates A and A' are plotted), as a function of Q, for a perturbation $b/\epsilon = 0.5$ (right panel), and the value of Q corresponding to the maximum of $\langle A' \rangle$ (the corresponding Q for the uncorrected coordinate $\langle A \rangle$ is also shown). Interestingly, the peak in the average number of nonnative contacts is detected for a value of Q corresponding to a pretransition state stage of the folding. A pre-TS peak is observed in both theory and simulations, although in the theory it is closer to the unfolded state than what is detected in simulations (see Figs. 6B and 7A).

Figures 6 and 7 present a thorough comparison between the allowed and most probable values for the fraction of nonnative contacts at different stages of the folding, as obtained from theory and simulations. Although the maximum number of nonnative contacts is always detected in a pre-TS region, independently on the value of b/ϵ, it is clear from Figures 6A and 7A that larger values of b/ϵ yield a larger number of nonnative contacts formed, particularly in the unfolded ensemble. Interestingly, however, the number of nonnative interactions rapidly decreases to zero in regions with very small Q. The cause of this effect is not contained in the analytical expressions 7c, where it is assumed that $A_{max} = 1 - Q$. This result is caused partly by coupling between nonnative contacts and the angle and dihedral terms in the simulation Hamiltonian (which are not present in the theory). This is a finite size effect that tends to increase the polymer stiffness relative to that in the theory, which used a bulk approximation for thermodynamic quantities. Compact states with $\eta \sim 1$ in which only nonnative interactions are present have large energetic cost and are formed very rarely. Another source of this effect is that forming collapsed conformations induces some native contacts to be formed, owing to the finite range of interactions. This effect is particularly important for short-range contacts among residues closely separated in sequence, and does not necessarily go away as one considers larger-size systems. This is the complementary effect to the already mentioned fact that in simulations nonnative interactions are formed in the native state (that has led us to a redefinition of the simulation reaction coordinate A').

To quantify this effect, we have generated a large (50) set of nonnative energy distributions with high and very high variance ($b/\epsilon \geq 2$ and $b/\epsilon \gg 2$). Sequences with these high values of b/ϵ are not able to fold to the selected native structure, but are useful to explore the region of the configurational space corresponding to compact structures with the maximum number of nonnative contacts formed. We expect the glass temperature of these sequences to be higher than their folding temperature (see the next section). After an initialization at very high temperature ($T \gg T_f^\circ$), a large number (>1000) of quenching simulations ($T \ll T_f^\circ$) has been performed for each sequence to generate a representative sample of compact misfolded structures. The maximum fraction of nonnative contacts that can be formed,
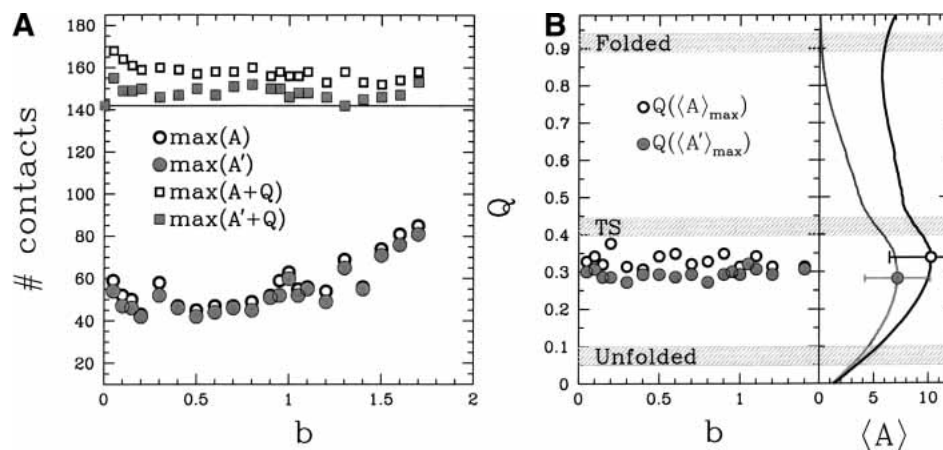
Figure 6. (*A, lower* panel) The maximum number of nonnative contacts registered in simulations for different values of the perturbation parameter *b* (in units of ε). Open circles indicate the maximum in the reaction coordinate *A*, whereas filled gray circles correspond to the corrected coordinate *A'* (see text for details). (*Upper* panel) The maximum number of all contacts (both native and nonnative) for different values of *b*. Open squares indicate the maximum value obtained when all contacts separated by at least three residues along the sequence are considered (i.e., *Q* + *A*); filled gray squares correspond to the values obtained when nonnative contacts likely to be formed in the native structure are removed (i.e., *Q* + *A'*). (*B, right* panel) Average number of nonnative contacts ⟨*A*⟩ formed in simulations as a function of the number of native contacts formed, for a perturbation parameter *b*/ε = 0.5. Horizontal bars at the maximum of ⟨*A*⟩ correspond to the standard deviation around the average at the peak value. The black curve corresponds to the coordinate *A*, and the gray line to *A'*. (*Left* panel) The values of *Q* corresponding to the maximum of ⟨*A*⟩ and ⟨*A'*⟩ for different values of the perturbation parameter *b* (open circles and filled gray circles, respectively).

A'_{max}, is thus defined as the largest values of *A'* among the vast pool of structures obtained by adding the results from the quenching simulations for high *b*/ε values to all con-figurations collected in simulations at any temperature and for any value of *b*/ε used in this study. Figure 7B shows the behavior of A'_{max} as a function of the fraction of native
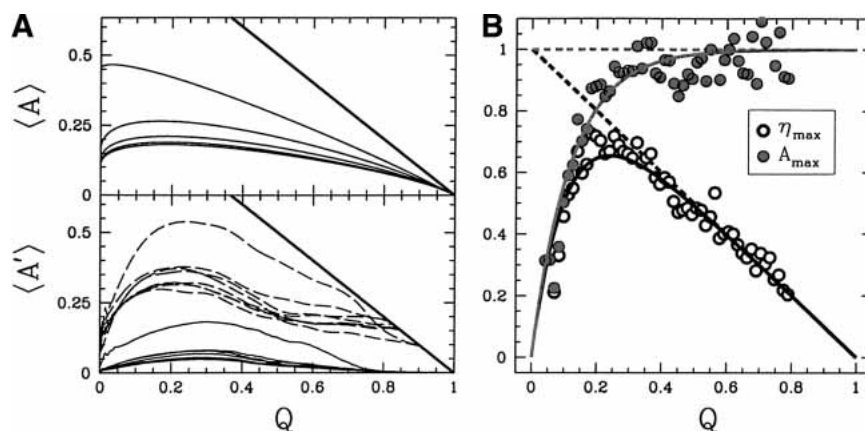
Figure 7. (*A, upper* panel) Continuous curves illustrate the behavior of ⟨*A*⟩ versus *Q* as predicted by the theory (with all parameters set to the simulation values; see Table 1). The different curves correspond to values of *b*/ε = 0.1, 0.3, 0.5, 0.7, 0.9 (increasing values of *b* lead to higher values of ⟨*A*⟩). The thick black line represents the maximum value of *A* allowed in the theory at different values of *Q* (independent of the value *b*). (*Lower* panel) ⟨*A'*⟩ vs. *Q* (continuous curves) as obtained from simulations, for values of *b*/ε = [0.2, 1.6] (increasing values of *b* lead to higher values of ⟨*A'*⟩). Dotted curves represent the highest values of *A'* found in simulations at different values of *Q*, for the same values of *b*/ε. The maximum value of *A* allowed in the theory is also plotted for comparison (thick black line). (*B*) Filled gray circles show the maximum value of *A'* detected in all equilibrium and quenched simulations for many values of *b* (see text), as a function of the fraction of native contacts formed, *Q*. Open circles correspond to the maximum packing fraction of the nonnative part of the protein, as obtained by using equation A.1 in the Supplemental Material, that is, $\eta_{max} = A'_{max}/(1 - Q)$. Dotted lines show the maximum values for *A* (in black) and η (in gray) allowed in the theory. Continuous lines in the corresponding colors represent the best fit of the data to a phenomenological exponential decay of A'_{max} at small values of *Q*: $A'_{max} = (1 - Q)[1 - \exp(-Q/Q_c)]$. Regression analysis yields $Q_c = 0.12$. The best fit for A'_{max} is shown in gray, and in black for η_{max}.

contacts present in the structures. The theoretical assumption on the maximum fraction of nonnative contacts $A_{\max} = 1 - Q$ holds remarkably well up to the values of $Q \lesssim 0.15$ that correspond to the unfolded state minimum in the free energy landscape (see Fig. 1). From these results, we then expect the unfolded region of a free energy landscape associated with the simulated protein Hamiltonian to be somewhat compressed toward smaller values of A with respect to the theoretical prediction.

Energy, entropy, and free energy landscape

Figure 1 presents the energy, entropy, and free energy profiles obtained from simulations, as a function of the reaction coordinates Q and A', for three different values of the perturbation parameter b/ϵ. The corresponding quantities obtained from the analytical theory, with all the parameters set equal to the simulations parameters (i.e., rightmost column in Table 1) and $b = 0.3\epsilon$, is also shown for comparison. For a more direct comparison with the results from simulations, the thermodynamic quantities from theory are only plotted in regions populated with probability $>2 \times 10^{-7}$, as we have typical samplings of ~5×10^6 configurations in folding/unfolding simulations. It is apparent from Figure 1 that the region of the (Q,A') space populated with high probability in simulations differs somewhat from the (Q,A) region predicted by theory. Several factors are responsible for this difference and have to be considered before one tests the predictive power of the theory with the simulation results:

1. The unperturbed energy function used in simulations includes a self-avoiding term for all nonnative contacts, which is maintained in the perturbed Hamiltonian (see equations D.32 and D.33 in the Supplemental Material). This energy term is not explicitly considered in the

theory. The short-distance repulsive interactions limit the formation of nonnative contacts (especially for small values of b/ϵ), and shifts the most populated regions of the folding landscape toward lower values of A. This effect also accounts for most of the differences in the energy landscape between theory and simulation results (see Fig. 1).

2. The analytic expressions are obtained in the thermodynamic limit, whereas simulations are performed for a small protein (57 residues). The theoretical expressions do not explicitly keep track of finite-size effects due to polymer stiffness. However, the extra effect of polymer stiffness seen in the simulations only enhances the theoretically predicted rate acceleration effect (see below).

3. The functional form for the entropy is approximated in the theory, and it is not expected to quantitatively reproduce the simulation results exactly. Particularly, the theoretical assumption on the allowed values of A at different Q (i.e., equation A.1 in the Supplemental Material) directly enters the derivation of the entropy (see Supplemental Material for details), and contributes to the relative "distortion" of the theoretical free energy landscape with respect to the landscape in the simulations. Nevertheless, the overall qualitative behavior of the entropy is correctly captured by the theory (see third column of Fig. 1).

4. The position of the folded and unfolded free energy minima emerging from simulation data differs from $Q = 0$ and $Q = 1$, as assumed in the theory (see above).

Overall, the destabilization of the folding free energy landscape upon introduction of nonnative energy perturbation is strongly reduced in simulations with respect to what is predicted by the theory. In fact, although in the theory a perturbation of $b/\epsilon \sim 1$ renders a protein unfoldable (i.e., $T_f/T_g \sim 1$; see equation 21 and Plotkin 2001), it is found in simulations that all sequences generated with a perturbation parameter $b/\epsilon \lesssim 1.7$ (entering the Hamiltonian, equation D.33 in the Supplemental Material) are able to reversibly fold/unfold at the Gō transition temperature T_f°. The next section quantifies this difference in the destabilization of the folding mechanism by comparing the folding and glass temperatures computed in simulations with their corresponding theoretical predictions.

Folding temperature and glass temperature

The folding temperature T_f of each protein model is estimated in simulations as the temperature corresponding to the peak in the specific heat curve (see Fig. 8A). This value is in good agreement (within the error bars) with the value obtained from the alternative definition of T_f as the tem-

Table 1. *Table of values for parameters in the model*

Symbol	Meaning	Equation[a]	Simulation values
N	Total number of residues in the protein	1	57
M	Total contacts in a fully collapsed globule	1	142
z	Average number of contacts per residue	1	2.49
ϵ	Native energy per contact	1	−1.0
E_N	Energy in the native state	1	−142.0
$\ln\nu$	Maximal entropy per residue	A.2	~2.4
ϵ_{NN}	Mean energy of nonnative contacts	6, 7a	0.0
b^2	Energetic variance of nonnative contacts	6, 7a	[0.0–4]
T_F^o	Gō folding temperature (in energy units)	11	~1.07

[a] Equation where the symbol is first defined, or representative equation.
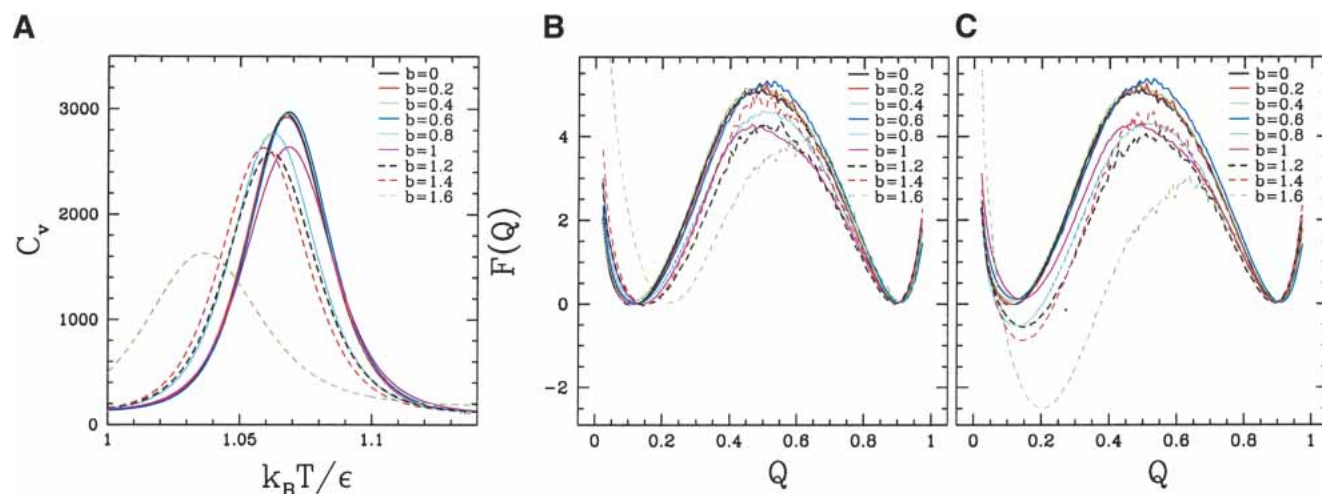
Figure 8. (*A*) Heat capacity as a function of temperature, as obtained from simulations for different values of the parameter *b*. Temperature is measured in units of native energy per contact, ϵ. (*B*) Free energy as a function of the fraction *Q* of native contacts, as obtained from simulations for several different values of the nonnative energy perturbation parameter *b*. Free energy curves for all values of *b* shown in *B* are obtained at their corresponding folding temperatures $T_f(b)$ (estimated from the heat capacity curves, plotted in *A*), whereas all curves in *C* are at the folding temperature of the unperturbed case $T_f^\circ = T_f(b = 0)$.

perature at which the folding and unfolding states have the same free energy (see Fig. 8B).

From equation 7c, upon increasing nonnative interaction strength (increasing *b*, and/or increasing $|\epsilon_{NN}|$ with $\epsilon_{NN} < 0$), the free energy $F(Q)$ lowers with respect to the Gō free energy at fixed temperature $T = T_F^\circ$. During this change of Hamiltonian, the free energy of the native structure remains roughly constant at E_N (see Fig. 8C). Even though the unfolded state is stabilized with respect to the folded state during the process of increasing nonnative interaction strength at fixed temperature, the folding rate nevertheless accelerates, because the free energy of the transition state lowers more than the unfolded state does. This is described in more detail below, with the result shown in Figure 10B.

The thermodynamic glass temperature T_g can be estimated by using the results obtained in the framework of the random energy model (REM; Derrida 1981; Bryngelson and Wolynes 1987). As the energetic frustration of the system arises from randomly assigned nonnative interactions, we assume that the energy of compact (misfolded) structures in the unfolded ensemble is Gaussianly distributed, with mean value $\langle E_{nn}(Q_u) \rangle = MA_{max}\epsilon_{NN}$ and variance $\delta E_{nn}^2(Q_u) = b^2 A_{max} M$, where MA_{max} is the maximum number of nonnative contacts the protein can form. In the theory, the maximum number of nonnative contacts was approximated at $Q \sim 0$ as the total number of native contacts $MA_{max} = M$. As we have already discussed above, the actual maximum number of nonnative contacts detected in simulations is smaller than the theoretical value, and it is expected to (slightly) vary with different realizations of the nonnative noise (see Fig. 6).

The REM glass temperature is defined by the vanishing of the thermal entropy (Derrida 1981; Bryngelson and Wolynes 1987), which corresponds to setting equation 7b to 0:

$$S(Q_u, A_{max}, T_g) = Ns_c(Q_u, A_{max}) - \frac{MA_{max}b^2}{2T_g^2} = 0. \qquad (20)$$

However, here we let A_{max} be a new parameter. This gives for the glass temperature:

$$T_g = b\sqrt{\frac{zA_{max}}{2s_c}} = \frac{\delta E_{nn}(Q_u)}{\sqrt{2Ns_c}} \qquad (21)$$

where $\delta E_{nn}(Q_u) = MA_{max}b^2$ is the energetic variance over the set of misfolded structures. For each protein model (i.e., each value of b/ϵ), we have performed several (>500) short quenching simulations to explore the compact configurations in the unfolded ensemble. A different open configuration is initially created by means of ancillary high-temperature simulations (with $T \gg T_f$), then rapidly quenched to very low temperatures ($T \sim T_f/10$, $T \sim T_f/25$, and $T \sim T_f/50$). The fluctuations of the nonnative energy in the compact misfolded configurations recorded during the quenching simulations are used to compute $\delta E_{nn}(Q_u)$ entering expression 21.

Figure 9A shows the folding temperature T_f and the glass temperature T_g obtained from simulation, as a function of the strength of the nonnative energy perturbation, *b* (in units of the native energy per contact, ϵ). The folding temperature

Figure 9. (*A*) Folding temperature T_f (open circles) and glass temperature T_g (filled gray circles), from simulation of the perturbed Gō model, as a function of the nonnative energy perturbation strength b (with $\epsilon_{NN} = 0$). Dotted lines represent the theoretical prediction for T_f (black line) and T_g (gray line), when all the parameters of the theory are set equal to the simulation parameters (see Table 1). Dashed lines represent the best fit of the simulation data to the theoretical prediction (see *B*). Temperatures and energies are measured in units of ϵ, the native energy per contact. The folding temperature is almost constant in the range shown, while the glass temperature rises from 0 (plain Gō model, with no energetic frustration), to values close to T_f for a high level of nonnative perturbation. As T_g/T_f approaches 1, several nonnative low-energy states compete with the native state and the folding is dramatically slowed down. Moreover, as $T_g/T_f \to 1$, the system is no longer self-averaging, and different realizations of the nonnative perturbation can lead to different results. There is a wider range where $T_f/T_g > 1$ in the simulations than in the theory, indicating a larger range of b where rate enhancement effects may be seen. (*B*) The same destabilizing effect on the folding predicted in the theory (in terms of T_f/T_g), for a given value of the parameter b, is observed in simulations for a much larger value of b. All values of b used in simulations (b_{sim}) are plotted in this figure as a function of the values of b yielding the same glass temperature in the theory (b_{theory}; see text for details). The dashed line represents the best fit of the data to the expression $b_{sim} = \alpha b_{theory} + \beta$, for $b_{sim} > 0.8$. The result from this fit is also shown in *A*.

is almost constant in the range shown, while the glass temperature rises from zero ($b = 0$ corresponds to the plain Gō-like model with no energetic frustration; see equation D.3 in the Supplemental Material), to values close to T_f for large nonnative perturbations ($b \gtrsim 1.6$). When $T_g/T_f \approx 1$, many low-energy misfolded structures compete with the native state, and folding is dramatically slowed down. As the ratio T_g/T_f increases beyond unity, the system is no longer self-averaging, and different realizations of the nonnative perturbation can lead to different folding mechanisms consistent with the same native topology. This point is discussed in a separate publication (S.S. Plotkin and C. Clementi, unpubl.). The glass temperature predicted by the theory for different values of b is also obtained from equation 21, with $\delta E_u^2 = MA_{max}(Q_u)$, $MA_{max}(Q) = M(1 - Q)$, and Q_u corresponding to the unfolded free energy minimum at T_g. The theoretical folding temperature is evaluated as described above. The comparison of the folding and glass temperatures from simulation with the corresponding values predicted by the theory (dotted curves in Fig. 9A) clearly shows that the destabilizing effect of the nonnative energy perturbation on the folding process (quantified by the ratio T_g/T_f) is much reduced in simulations with respect to the theoretical prediction. Each value of b used in simulations (b_{sim}) is plotted in Figure 9B as a function of the value of b

used in the theory (b_{theory}) that yields the same T_g. The corresponding $T_f(b_{sim})$ (from simulation) and $T_f(b_{theory})$ (from theory) are also found equal within the error bar.

Folding rate enhancement/depression upon nonnative energy perturbation

The theoretical prediction on folding rate enhancement upon small nonnative energy perturbation is expected to hold for values of b with a corresponding small ratio T_g/T_f. A perturbation that largely increases the ratio T_g/T_f will also largely decrease the prefactor k_0 in equation 19, and folding then slows (see discussion above). Because of the extended range of b for which the condition $T_g/T_f \ll 1$ remains valid in simulations (see previous section), we expect to detect a rate enhancement in simulations up to values of $b \sim 1$; that is, the theory is conservative in that rate is enhanced over a wider range of b in the simulations.

We have shown in the previous section that the analytical theory reproduces correctly, at a qualitative level, the thermodynamics quantities measured in simulations, although we have highlighted some quantitative differences. The effect of these differences on equation 16, which predicts the rate enhancement, is expected to be confined to the precise evaluation of the difference in the number of nonnative

contacts between the transition state and unfolded state, $\Delta A^{\neq} \equiv \Delta A^*(Q^{\neq})$, and to a lesser extent the precise positions of the transition state and unfolded state, $Q^{\ddagger}$ and Q_u, respectively. Equation 16 can thus be directly and quantitatively tested if $\Delta A^*(Q^{\neq})$ is evaluated from simulation. Figure 10A shows the difference $M(\langle A' \rangle_{TS} - \langle A' \rangle_U) \equiv M\Delta A'^{\neq}$ between the average number of nonnative contacts $M\langle A' \rangle_{TS}$, formed in the simulated transition state ensemble, and the average $M\langle A' \rangle_U$, formed in the simulated unfolded ensemble. This number slightly varies over the range of b values where we expect to find the rate enhancement effect ($T_g/T_f \lesssim 0.25$ up to $b \lesssim 1.3\epsilon$). Because the variation of $M\Delta A'^{\neq}$ with b in this range is smaller than the error bar associated to it, we consider its average over the different b values (straight black line in Fig. 10A). This average value is then used in equation 16; the resulting quantity $\ln(k/k_o) = (\Delta F_0^{\neq} - \Delta F^{\neq})/T_F^{\circ}$ is compared with the difference in log folding rate estimated directly from a large set of folding simulations. Figure 10B shows that the agreement between the values predicted from equation 16 (dashed black line) and simulation results for the rate (filled gray circles) and barrier height (open circles) is, indeed, remarkably good up to $b \lesssim 1 - 1.1$.

Folding rates obtained from simulations performed with $b = 0$ and variable ϵ_{NN} are also plotted in Figure 10C. As predicted by the theory, rates accelerate when $\epsilon_{NN} < 0$ (attractive nonnative interactions) and decelerate when $\epsilon_{NN} > 0$ (repulsive nonnative interactions). The theory gives excellent agreement with the simulations in the perturbative limit (dashed line in Fig. 10C). The effect on the rate (at T_f°) of a perturbation with $(b, \epsilon_{NN}) = (0, -b^2/2T_F^{\circ})$ is equivalent to the case with $(b, \epsilon_{NN}) = (b, 0)$. When ϵ_{NN} becomes sufficiently attractive, the prefactor becomes increasingly important in determining the folding rate, and rates begin to decrease dramatically.

Conclusions

In this paper, we derived a theory for the change in the free energy barrier height to protein folding, as the strength of nonnative interactions is varied. We find that the barrier height initially decreases as the strength of nonnative interactions increases.

This means that if one considers two idealized protein sequences, one completely unfrustrated (a so-called Gō-like protein) and one with weak nonnative interactions that are either attractive or randomly distributed, the mildly frustrated protein will tend to fold faster at the same temperature, particularly when the temperature is near the transition temperature of the Gō protein. This result follows from energy landscape theory (Plotkin 2001).

The criterion for the rate to increase is related to an increase in packing fraction in the transition state relative to the unfolded state (equation 18).
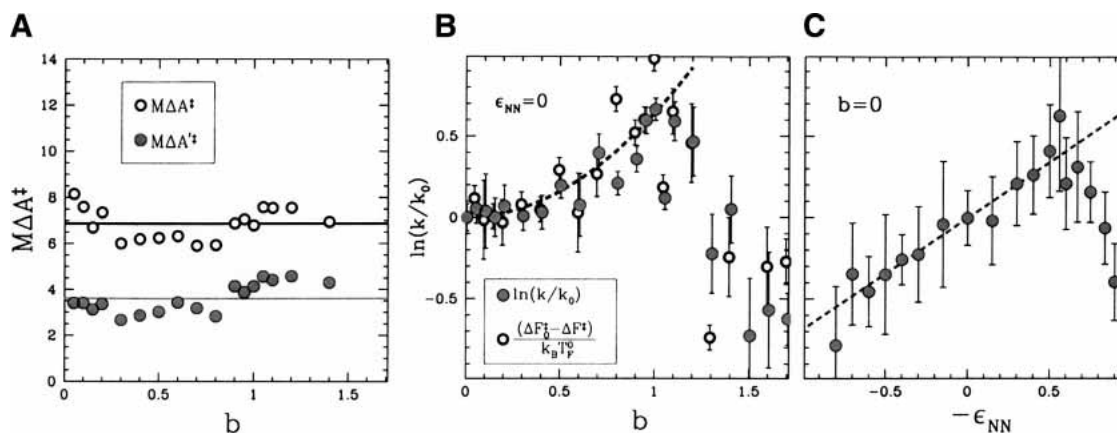
Figure 10. (*A*) Average difference in the number of nonnative contacts in the transition state and unfolded state ensemble, as detected from simulation, as a function of the perturbation parameter b/ϵ. The values obtained by considering all nonnative contacts are shown as open circles, whereas filled gray circles correspond to the corrected values (i.e., considering only nonnative contacts that are not formed in the folded state; see text for details). The average of these quantities over all the considered values of b/ϵ are plotted as continuous straight lines of the same color. These numbers are comparable to the theoretical estimates of approximately six more nonnative contacts in the transition state for a 100-residue protein (see Fig. 4). (*B*) Barrier height $\Delta F\dagger$ (open circles) and log folding rate k (filled gray circles) as a function of the nonnative energy perturbation strength b (for $\epsilon_{NN} = 0$), and (*C*) log folding rate k as a function of the average nonnative energy ϵ_{NN} (for $b = 0$). The parameters controlling the strength of the nonnative energy, $b^2/2T$ and ϵ_{NN}, enter the free energy at the same footing in the theoretical model (see equation 7c). Results from simulations are in very good agreement with the theoretical prediction (dashed black curve in B and C) obtained when the value of $\Delta A'^{\neq}$—shown in A—is used as an estimate of $\Delta A^{\neq} \equiv \Delta A^*(Q^{\neq})$ entering equation 16 predicted by the theory. Values of $\ln k$ and $\Delta F\dagger$ are normalized to the corresponding values for the unperturbed case ($\ln k_0$ and $\Delta F_0\dagger$). For large nonnative energy perturbations ($b > 1$, or $\epsilon_{NN} > 0.5$), both $\Delta F\dagger(T_f^{\circ})$ and $\ln k$ rapidly decrease (see also Figure 8B,C). The energy parameters b and ϵ_{NN} are measured in units of native energy per contact, ϵ. Barrier heights are measured in units of the folding temperature for the unperturbed case ($k_B T_0$).

The rate increase is supported by the theoretical proposal that proteins exhibit a dynamic glass transition at nonzero temperature. The consequence of this is that the prefactor to the rate is initially unaffected as nonnative interactions are increased in strength from zero. Thus, rate-determining effects for nearly unfrustrated proteins arise largely from effects on the folding barrier.

Off-lattice simulations of a coarse-grained C_α model of src-SH3 were used to test the theoretical predictions. Simulation results showed even more robust rate-enhancement effects than the theory, owing essentially to chain stiffness and contact range effects that decrease the number of nonnative interactions in the unfolded state. When these corrections are included, theory and simulations are in very good agreement (Fig. 10).

The experimental relevance of this effect (reduced number of nonnative contacts in the unfolded state) depends on whether the fraction of native contacts formed, Q, is a good reaction coordinate for these systems. For unfrustrated or nearly unfrustrated systems, Q has been shown to work well as a reaction coordinate in lattice models (Nymeyer et al. 2000; lattice models have limited move-sets that may further hinder the use of Q as a reaction coordinate, relative to the off-lattice system we studied here), and off-lattice Gō-like models of short proteins (Shea et al. 2000; Clementi et al. 2001).

Random nonnative interactions as well as attractive nonnative interactions both speed the folding rate, when they are perturbatively small compared with the large native interaction energies that drive folding. The analysis here was done at the transition temperature of the Gō model. Because the coupling of collapse with folding is fairly generic, it is expected that the effect of rate-enhancement would also be seen at different temperatures and stabilities.

The effect of rate enhancement by nonnative stabilization has been seen in several simulation models (Li et al. 2000; Cieplak and Hoang 2002; Fan et al. 2002; Treptow et al. 2002), as well as experiments involving the strengthening of nonspecific hydrophobic interactions in α-spectrin SH3 (Viguera et al. 2002).

Some proteins are thought to be sufficiently frustrated that nonnative interactions may limit the folding rate. These proteins would have nonnative energy scales somewhat larger than unity in Figure 10B, at least for some nonnative contacts. In some proteins such as lysozyme, these nonnative interactions are thought to stabilize early-formed structures to prevent degradation or aggregation (Klein-Seetharaman et al. 2002). All-atom simulations of the 36-residue villin headpiece segment suggested that the breaking of nonnative interactions incorrectly packed in the hydrophobic core may form the rate-limiting step on some folding trajectories (Zagrovic et al. 2002; the authors caution, however, that this may indicate frustration in villin, or may indicate an artifact of the forcefield used). For proteins that must escape kinetic traps to fold, it is possible that other evolutionary mechanisms in addition to funneling may assist folding, such as the selection for amino acids that reduce the escape barrier from the trap (Plotkin and Wolynes 2003).

To quantify the rate enhancement, it was necessary to treat the entropy of a finite-sized, self-avoiding chain—a problem of some interest to polymer physics. The mean-field Flory entropy of a long, self-avoiding chain of packing fraction η must be modified when the chain is sufficiently short that configurations with the characteristic radius of gyration have nonzero packing fraction. Then most states have a finite packing fraction dependent on the length of the chain, rather than the bulk value of zero.

From the analysis of simulation data and its comparison with the theory, it emerges that nonnative perturbations up to values of $b \sim \epsilon$ yield values of $T_g/T_f \lesssim 0.4$ (see Fig. 9), that can still be considered realistic for proteins. All sequences characterized by this range of frustration are fast-folders; however, the range of ruggedness is sufficiently wide that a variety of scenarios are possible a priori for the folding rate. Both rate enhancement and reduction are compatible for realistic levels of frustration. This fact may have been exploited by natural evolution to select different effects for different purposes (in the same structural family). It is worth noticing that the observed rate enhancement/reduction induced by nonnative interactions is limited to less than an order of magnitude (at least for the SH3 fold considered here); thus, it cannot be used to explain the much larger variation (spanning more than six orders of magnitude) of folding rates experimentally observed for single-domain, two-state folding proteins (Plaxco et al. 1998, 2000b).

In this paper, we made a very simple generalization of the Gō Hamiltonian for a foldable protein, and found this resulted in nontrivial and rich behavior of the dynamics of the system. It will be interesting to see what new phenomena emerge from further considerations of the Hamiltonian describing biomolecular folding and function.

Acknowledgments

payment of page charges. This article must therefore be hereby marked "advertisement" in accordance with 18 USC section 1734 solely to indicate this fact.

References

Alm, E. and Baker, D. 1999. Prediction of protein-folding mechanisms from free-energy landscapes derived from native structures. *Proc. Natl. Acad. Sci.* **96:** 11305–11310.

Baker, D. 2000. A surprising simplicity to protein folding. *Nature* **405:** 39–42.

Berendsen, H.J.C., Postma, J.P.M., van Gunsteren, W.F., DiNola, A., and Haak, J.R. 1984. Molecular dynamics with coupling to an external bath. *J. Chem. Phys.* **81:** 3684–3690.

Bryngelson, J.D. and Wolynes, P.G. 1987. Spin glasses and the statistical mechanics of protein folding. *Proc. Natl. Acad. Sci.* **84:** 7524–7528.

Bryngelson, J.D., Onuchic, J.N., Socci, N.D., and Wolynes, P.G. 1995. Funnels, pathways and the energy landscape of protein folding. *Proteins* **21:** 167–195.

Cieplak, M. and Hoang, T.X. 2002. The range of the contact interactions and the kinetics of the Gō models of proteins. *Int. J. Mod. Phys. C* **13:** 1231–1242.

Clementi, C., Jennings, P.A., and Onuchic, J.N. 2000a. How native state topology affects the folding of dihydrofolate reductase and interleukin-1β. *Proc. Natl. Acad. Sci.* **97:** 5871–5876.

Clementi, C., Nymeyer, H., and Onuchic, J.N. 2000b. Topological and energetic factors: What determines the structural details of the transition state ensemble and "en-route" intermediates for protein folding? An investigation for small globular proteins. *J. Mol. Biol.* **298:** 937–953.

Clementi, C., Jennings, P.A., and Onuchic, J.N. 2001. Prediction of folding mechanism for circular-permuted proteins. *J. Mol. Biol.* **311:** 879–890.

Clementi, C., Garcia, A.E., and Onuchic, J.N. 2003. Interplay among tertiary contacts, secondary structure formation and side-chain packing in the protein folding mechanism: An all-atom representation study. *J. Mol. Biol.* **326:** 933–954.

Creighton, T.E. 2002. *Proteins: Structure and molecular properties.* W.H. Freeman, New York.

Derrida, B. 1981. Random-energy model: An exactly solvable model of disordered systems. *Phys. Rev. B* **24:** 2613–2626.

Eastwood, M.P. and Wolynes, P.G. 2001. Role of explicitly cooperative interactions in protein folding funnels: A simulation study. *Proteins* **30:** 215–227.

Ervin, J. and Gruebele, M. 2002. Quantifying protein folding transition states with $\Phi(T)$. *J. Biol. Phys.* **28:** 115–128.

Fan, K., Wang, J., and Wang, W. 2002. Folding of lattice protein chains with modified Gō potential. *Eur. Phys. J. B* **30:** 381–391.

Ferguson, N., Capaldi, A.P., James, R., Kleanthous, C., and Radford, S.E. 1999. Rapid folding with and without populated intermediates in the homologous four-helix proteins Im7 and Im9. *J. Mol. Biol.* **286:** 1597–1608.

Ferrenberg, A.M. and Swendsen, R.H. 1988. New Monte Carlo technique for studying phase transitions. *Phys. Rev. Lett.* **61:** 2635–2638.

———. 1989. Optimized Monte Carlo data analysis. *Phys. Rev. Lett.* **63:** 1195–1198.

Fersht, A.L. 2000. *Structure and mechanism in protein science: A guide to enzyme catalysis and protein folding.* W.H. Freeman, New York.

Fersht, A., Leatherbarrow, R., and Wells, T. 1986. Quantitative analysis of structural activity relationship in engineered proteins by linear free energy relationships. *Nature* **322:** 284–286.

Finkelstein, A.V. and Badretdinov, A.Y. 1997. Rate of protein folding near the point of thermodynamic equilibrium between the coil and the most stable chain fold. *Fold. Des.* **2:** 115–121.

Flory, P.J. 1953. *Principles of polymer chemistry.* Cornell University Press, Ithaca, NY.

Galzitskaya, O.V. and Finkelstein, A.V. 1999. A theoretical search for folding/unfolding nuclei in three-dimensional protein structures. *Proc. Natl. Acad. Sci.* **96:** 11299–11304.

Goldstein, R.A., Luthey-Schulten, Z.A., and Wolynes, P.G. 1992. Optimal protein-folding codes from spin-glass theory. *Proc. Natl. Acad. Sci.* **89:** 4918–4922.

Gruebele, M. 1999. The fast protein folding problem. *Annu. Rev. Phys. Chem.* **50:** 485–516.

Gunasekaran, K., Eysel, S., Hagler, A., and Gierash, L. 2001. Keeping it in the family: Folding studies of related proteins. *Curr. Opin. Struct. Biol.* **11:** 83–93.

Honeycutt, J. and Thirumalai, D. 1992. The nature of the folded state of globular proteins. *Biopolymers* **32:** 695–709.

Karanicolas, J. and Brooks, C. 2003. The structural basis for biphasic kinetics in the folding of the WW domain from a formin-binding protein: Lessons for protein design? *Proc. Natl. Acad. Sci.* **100:** 3954–3959.

Kaya, H. and Chan, H.S. 2003. Solvation effects and driving forces for protein thermodynamic and kinetic cooperativity: How adequate is native-centric topological modeling? *J. Mol. Biol.* **326:** 911–931.

Kim, D.E., Fisher, C., and Baker, D. 2000. A breakdown of symmetry in the folding transition state of protein L. *J. Mol. Biol.* **298:** 971–984.

Klein-Seetharaman, J., Oikawa, M., Grimshaw, S.B., Wirmer, J., Duchardt, E., Ueda, T., Imoto, T., Smith, L.J., Dobson, C.M., and Schwalbe, H. 2002. Long-range interactions within a nonnative protein. *Science* **295:** 1719–1722.

Klimov, D. and Thirumalai, D. 1996. Criterion that determines the foldability of proteins. *Phys. Rev. Lett.* **76:** 4070–4073.

Kubelka, J., Eaton, W., and Hofrichter, J. 2003. Experimental tests of villin subdomain folding simulations. *J. Mol. Biol.* **329:** 625–630.

Lapidus, L.J., Eaton, W.A., and Hofrichter, J. 2000. Measuring the rate of intramolecular contact formation in polypeptides. *Proc. Natl. Acad. Sci.* **97:** 7220–7225.

Li, L., Mirny, L.A., and Shakhnovich, E.I. 2000. Kinetics, thermodynamics and evolution of non-native interactions in a protein folding nucleus. *Nat. Struct. Biol.* **7:** 336–342.

Matouschek, A., Kellis, J.T., Serrano, L., Bycroft, M., and Fersht, A.R. 1990. Transient folding intermediates characterized by protein engineering. *Nature* **346:** 440–445.

Mines, G.A., Pascher, T., Lee, S.C., Winkler, J.R., and Gray, H.B. 1996. Cytochrome *c* folding triggered by electron transfer. *Chem. Biol.* **3:** 491–497.

Munoz, V. and Eaton, W.A. 1999. A simple model for calculating the kinetics of protein folding from three-dimensional structures. *Proc. Natl. Acad. Sci.* **96:** 11311–11316.

Nymeyer, H., Socci, N.D., and Onuchic, J.N. 2000. Landscape approaches for determining the ensemble of folding transition states: Success and failure hinge on the degree of minimal frustration. *Proc. Natl. Acad. Sci.* **97:** 634–639.

Onuchic, J.N., Nymeyer, H., García, A.E., Chahine, J., and Socci, N.D. 2000. The energy landscape theory of protein folding: Insights into folding mechanisms and scenarios. *Adv. Protein Chem.* **53:** 87–152.

Paci, E., Vendruscolo, M., and Karplus, M. 2002. Validity of Gō models: Comparison with a solvent-shielded empirical energy decomposition. *Biophys. J.* **83:** 3032–3038.

Pande, V. 2003. Meeting halfway on the bridge between protein folding theory and experiment. *Proc. Natl. Acad. Sci.* **100:** 3555–3556.

Pearlman, D.A., Case, Caldwell, J.W., Ross, W.S., Cheatham, T.E., Ferguson, D.M., Singh, U.C., Weiner, P., and Kollman, P.A. 1995. AMBER. V. 4.1 University of California, San Francisco, CA.

Plaxco, K.W., Simons, K.T., and Baker, D. 1998. Contact order, transition state placement and the refolding rates of single domain proteins. *J. Mol. Biol.* **277:** 985–994.

Plaxco, K.W., Larson, S., Ruczinski, I., Riddle, D.S., Thayer, E.C., Buchwitz, B., Davidson, A.R., and Baker, D. 2000a. Evolutionary conservation in protein folding kinetics. *J. Mol. Biol.* **298:** 303–312.

Plaxco, K.W., Simons, K.T., Ruczinski, I., and Baker, D. 2000b. Topology, stability, sequence, and length: Defining the determinants of two-state protein folding kinetics. *Biochemistry* **39:** 11177–11183.

Plotkin, S.S. 2001. Speeding protein folding beyond the Gō model: How a little frustration sometimes helps. *Proteins* **45:** 337–345.

Plotkin, S.S. and Onuchic, J.N. 2002a. Understanding protein folding with energy landscape theory I: Basic concepts. *Q. Rev. Biophys.* **35:** 111–167.

———. 2002b. Understanding protein folding with energy landscape theory II: Quantitative aspects. *Q. Rev. Biophys.* **35:** 205–286.

Plotkin, S.S. and Wolynes, P.G. 2003. Buffed energy landscapes: Another solution to the kinetic paradoxes of protein folding. *Proc. Natl. Acad. Sci.* **100:** 4417–4422.

Sabelko, J., Ervin, J., and Gruebele, M. 1999. Observation of strange kinetics in protein folding. *Proc. Natl. Acad. Sci.* **96:** 6031–6036.

Sanchez, I.C. 1979. Phase transition behavior of the isolated polymer chain. *Macromolecules* **12:** 980–988.

Schuler, B., Lipman, E.A., and Eaton, W.A. 2002. Probing the free-energy surface for protein folding with single-molecule fluorescence spectroscopy. *Nature* **419:** 743–747.

Shea, J. and Brooks III, C. 2001. From folding theories to folding proteins: A review and assessment of simulation studies of protein folding and unfolding. *Ann. Rev. Phys. Chem.* **52:** 499–535.

Shea, J.E., Onuchic, J.N., and Brooks, C.L. 2000. Energetic frustration and the nature of the transition state in protein folding. *J. Chem. Phys.* **113:** 7663–7671.

Shimada, J. and Shakhnovich, E. 2002. The ensemble folding kinetics of protein G from an all-atom Monte Carlo simulation. *Proc. Natl. Acad. Sci.* **99:** 11175–11180.

Shoemaker, B.A., Wang, J., and Wolynes, P.G. 1997. Structural correlations in protein folding funnels. *Proc. Natl. Acad. Sci.* **94:** 777–782.

———. 1999. Exploring structures in protein folding funnels with free energy functionals: The transition state ensemble. *J. Mol. Biol.* **287:** 675–694.

Snow, C., Nguyen, H., Pande, V., and Gruebele, M. 2002. Absolute comparison of simulated and experimental protein-folding dynamics. *Nature* **420:** 102–106.

Sobolev, V., Wade, R., Vriend, G., and Edelman, M. 1996. Molecular docking using surface complementarity. *Proteins* **25:** 120–129.

Sorenson, J.M. and Head-Gordon, T. 2000. Matching simulation and experiment: A new simplified model for simulating protein folding. *J. Comput. Biol.* **7:** 469–481.

———. 2002. Protein engineering study of protein L by simulation. *J. Comput. Biol.* **9:** 35–54.

Takada, S., Portman, J.J., and Wolynes, P.G. 1997. An elementary mode cou-pling theory of random heteropolymer dynamics. *Proc. Natl. Acad. Sci.* **94:** 2318–2321.

Treptow, W.L., Barbosa, M.A.A., Barcia, L.G., and de Araújo, A.F.P. 2002. Non-native interactions, effective contact order, and protein folding: A mutational investigation with the energetically frustrated hydrophobic model. *Proteins* **49:** 167–180.

Ueda, Y., Taketomi, H., and Gō, N. 1975. Studies on protein folding, unfolding, and fluctuations by computer simulation. *Int. J. Peptide Protein Res.* **7:** 445–459.

Viguera, A.R., Vega, C., and Serrano, L. 2002. Unspecific hydrophobic stabilization of folding transition states. *Proc. Natl. Acad. Sci.* **99:** 5349–5354.

Wang, J., Plotkin, S.S., and Wolynes, P.G. 1997. Configurational diffusion on a locally connected correlated energy landscape; application to finite, random heteropolymers. *J. Phys. I France* **7:** 395–421.

Winkler, J.R. and Gray, H.R. 1998. Protein folding. *Acc. Chem. Res.* **31:** 798.

Zagrovic, B., Snow, C.D., Shirts, M.R., and Pande, V.S. 2002. Simulation of folding of a small α-helical protein in atomistic detail using worldwide-distributed computing. *J. Mol. Biol.* **323:** 927–937.